Prometheus Payload

Katie A. Blyler, Yasmine B. Kadire, Joseph E. Messner, Dylan L. Nastanski, Vraj P. Patel, Bryce A. Pochron[1]
The Pennsylvania State University, University Park, [1]PA, 16802, United States of America

Sara Lego[2]
The Pennsylvania State University, University Park, PA, 16802, United States of America

Michael Hernandez[3]
iMetalX, Sausalito, California, 94965, United States of America

The Prometheus mission demonstrates an in-space servicing, assembly, and manufacturing (ISAM) payload capable of semi-autonomous rendezvous and debris capture, laser-cutting, and welding, integrated with the VENUS X-Class Bus. Using robotic arms equipped with a modified Paton electron beam welder and a conceptual fiber laser cutter, the system demonstrates procedures necessary for structural repairs and material processing in orbit. Diverse types of analysis confirm feasibility: Finite Element Analysis validated structural integrity under 5g launch loads and a power budget was designed through MATLAB's eclipse simulations and SMAD principles to ensure mission operations within the 444W cap from the Bus. Trade studies were used in the selection of actuators, computers, the welding gun, the laser-cutter, and the robotic arms. The mission advances through five stages including orbit determination, semi-autonomous rendezvous and capture of debris, semi-autonomous precision laser-cutting, semi-autonomous welding, and a brief structural test for weld integrity and then concludes its mission and deorbits. By demonstrating scalable in-space repair workflows, Prometheus advances the technological readiness of ISAM tools critical to future orbital infrastructure and debris mitigation efforts.

[1] Student, Aerospace Engineering, AIAA Undergraduate Student Member
[2] Associate Teaching Professor, Aerospace Engineering
[3] Senior GNC Engineer: Space Systems Architect

I. Introduction

The growing presence of defunct and damaged satellites in orbit poses a significant challenge to sustainable space operations. The European Space Agency estimates that there are over 1.2 million space debris objects larger than 1 cm, each capable of causing catastrophic damage. This underscores the urgent need for autonomous satellite servicing [1].

Fully or semi-autonomous satellite servicing remains largely unachieved. The ability to rendezvous with and repair satellites without human intervention would enhance mission longevity, reduce space debris, and lower replacement costs. However, current technologies face limitations in guidance, navigation, and control (GNC), autonomy, power management, mechanical capability, and regulatory compliance.

Precise rendezvous and docking are particularly challenging, as servicing satellites must avoid destabilizing their targets while maintaining their own stability. Reactionary forces from docking and repairs further complicate control algorithms. Autonomous decision-making under uncertainty also remains an obstacle, as servicing satellites must adapt to unforeseen failures or target anomalies. Limited fault detection and self-repair capabilities restrict long-duration missions.

Robotic arms, essential for servicing, require substantial power for tasks such as welding and laser cutting. However, space-grade power converters are insufficient to meet these demands, and electron beam welding adds mass and complexity. Additionally, servicing systems must be adaptable to non-standardized satellite interfaces, as many older or foreign satellites lack uniform structural designs.

Regulatory and safety considerations further complicate deployment. Any unintended damage during servicing risks exacerbating the space debris problem. While technological advancements have addressed some aspects of autonomous satellite servicing, a fully capable system has yet to be realized.

II. Mission Overview

The Prometheus Mission payload is designed to demonstrate a suite of in-space servicing capabilities using semi-autonomous robotic manipulation. While there was a recent mission launched aimed to be one of the first autonomous in-space welding system, the Prometheus payload builds on that foundation by not only performing welding operations, but introduces laser cutting capabilities, further expanding the range of in-space servicing functions. Prometheus also incorporates a more intense debris mitigation strategy incorporated to the body of the payload, which is explained further in section III. Central to the mission is the ability to perform both welding and laser cutting operations in space, leveraging robotic arms to execute these tasks with minimal human intervention. In addition to material processing, the payload will showcase its capability to rendezvous with and capture space debris, providing proof-of-concept for orbital debris removal technologies. To support these primary functions, the robotic arms must also demonstrate dexterous control over debris and material, enabling precise handling and repositioning. Throughout all critical operations—welding, cutting, and capture—the system will semi-autonomously monitor performance and communicate results, ensuring operational awareness and enabling assessment of mission success. The payload will also include functionality to test the mechanical strength of welds, offering direct evaluation of structural integrity post-servicing. The payload is required to be hosted on the VENUS X-CLASS BUS, in accordance with specifications in the request for proposal (RFP) [2]. Furthermore, the mission must adhere to NASA's space debris mitigation guidelines (NPR 8715.6E), ensuring responsible on-orbit behavior and alignment with space sustainability practices.

To visualize the Prometheus mission concept, Figure 1 illustrates the macro-level mission architecture. The mission is structured around six generic steps which, if executed properly, will lead to a successful mission.

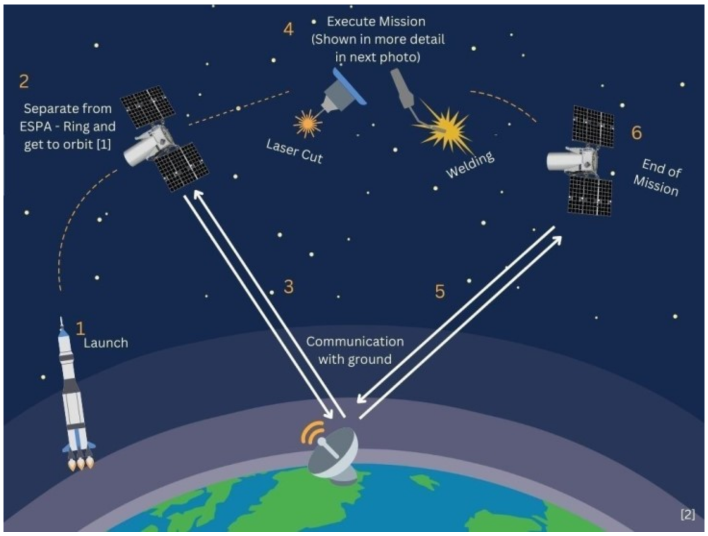

Figure 1. Macro-level Mission Architecture

The mission begins with launch, followed by separation from the launch vehicle-the choice of which will be discussed in a later section. Following separation, establishing communication with ground systems becomes critical, as it enables the payload to receive commands and status checks essential for the mission to operate in a semi-autonomous manner. Once communication is established, instructions will be uplinked to initiate an orbital maneuver that allows the payload to rendezvous with a targeted piece of space debris. This leads to the primary operations phase, including capture, welding, and laser cutting. More detail to be provided in the payload design section. Upon completion of these servicing tasks, new instructions will direct the payload to perform structural analysis of the welds by inducing loads on the welded structures. Finally, all collected data will be transmitted to ground stations for post-mission inspection and analysis.

III. Payload Design

The Prometheus Payload (shown in Figure 2) shows the deployed configuration of the payload. This figure points out the specific parts of the payload including the robotic arms (grabber and welding), welding panel, debris, and welding horn. This plate is attached to the payload by sleeves that grip onto the panel using geometry but are not completely attached. This allows for the plate to be removed if necessary for testing. During launch, the plate will be flush with the side of the payload and held down by the two clips shown in Figure 2, to ensure that the plate does not fold out during launch. Then by using linear actuators, the clips will move out of place to allow for the panel to rotate. By using servos, the panel will rotate 90 degrees, which will allow the spring pins to pop out locking the panel in place. The two robotic arms are then able to rotate around and touch the plate and complete the welding and laser cutting processes. The laser cutting will occur inside of the payload to mitigate debris. One arm will have a grabber at the end to grab the debris and the other arm will have a welding horn.

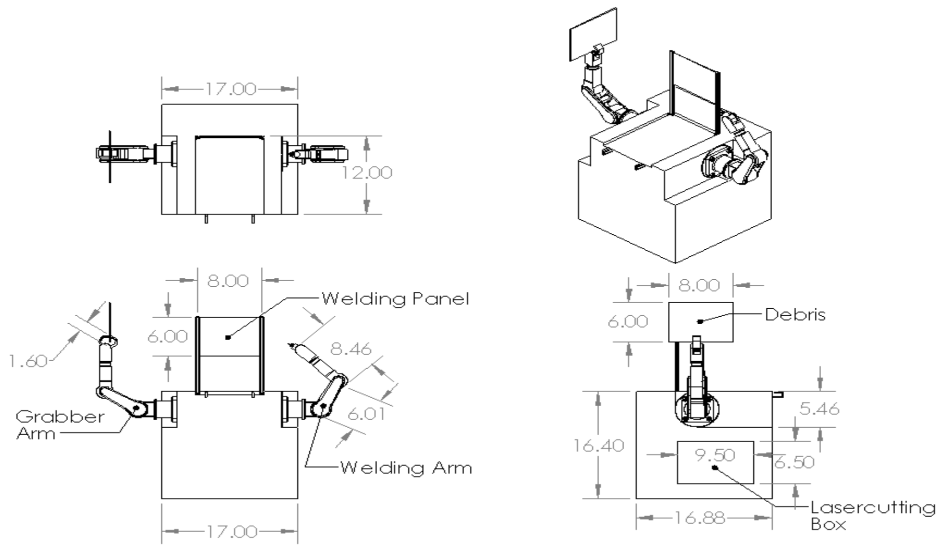

Figure 2. 3-View of the Prometheus Payload (dimensions in inches)

When the payload is in the configuration for launch, the panel will be flush with the body of the payload and the arms will be close to the body. When in the launch configuration, these dimensions satisfy the size constraints given in the RFP of 17" x 16.4" x 27" [2]. This can be seen in (b) of Figure 3. After achieving the intended orbit, the Prometheus payload will then begin deploying to the deployed configuration shown in Figure 2 and Figure 3.

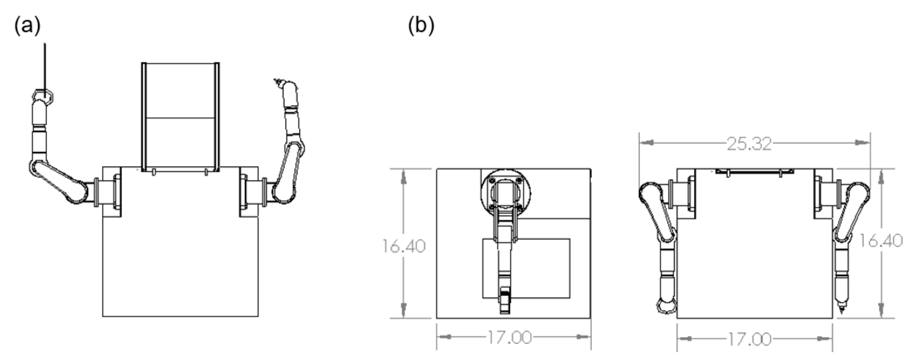

Figure 3. Deployed and Launch Configurations: (a) payload configuration once deployed and in use (b) payload configuration for launch (dimensions in inches)

The micro-level mission architecture for the Prometheus Mission (in Figure 4) begins after the payload reaches its intended orbit and (1) establishes communication with the ground station to confirm functionality and receive approval to start the mission. Once authorized, (2) the payload initiates a rendezvous procedure to capture the targeted space debris using a robotic arm equipped with a grabber hand. (3) The arm then puts the plate inside the hole on the side of the payload where the laser cutter is. The laser cutter then trims the debris to create a clean edge for welding. Next, (4) a folding arm deploys by removing a securing pin with linear actuators and rotating the panel 90º using rotary actuators, positioning the welding panel away from sensitive electronics to mitigate thermal risks while maintaining structural connection to the payload. (5) The robotic arm holding the debris aligns it with the folded plate, and a welding arm uses a high-velocity electron beam to fuse the plate and debris together by converting kinetic energy into heat. Following this, (6) structural analysis of the weld may be conducted by two robotic arms applying load and torque while measuring force, torque, and strain to ensure integrity. After data transmission to ground stations, (7) the robotic system retracts to its initial state and powers down.

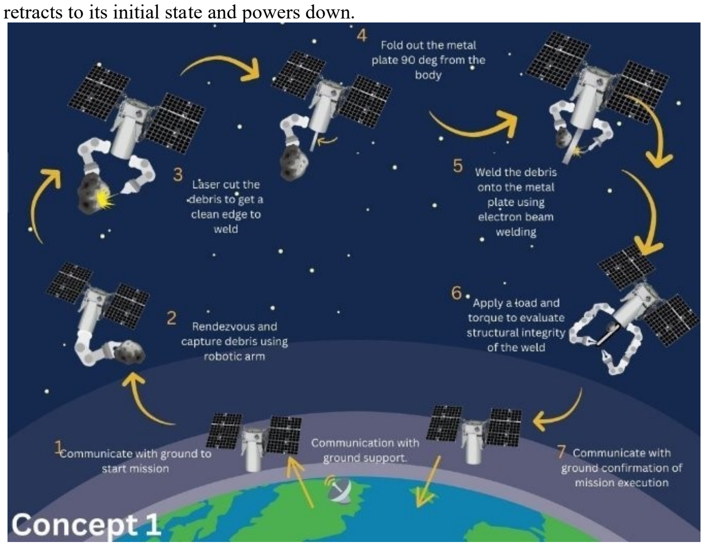

Figure 4. Micro-Level Mission Architecture for the Prometheus Payload

A. Electron Beam Welding

Electron Beam Welding (EBW) is a precise welding technique that uses a focused beam of electrons to join metals. It is well-suited for the space environment due to its ability to achieve pinpoint accuracy, making it ideal for intricate or confined areas. EBW produces deep, narrow welds with minimal distortion, ensuring dimensional stability in critical components. The process is typically performed in a vacuum to prevent contamination, which is a particular advantage of working in the space environment. Additionally, EBW is compatible with advanced materials like titanium and aluminum alloys, maintaining their integrity under extreme conditions. This combination of precision, minimal distortion, and material compatibility makes EBW a preferred choice for in- space applications.

The electron beam generation process begins with a cathode, typically made of materials like tungsten or lanthanum hexaboride, chosen for their low work function to allow easy electron extraction under high accelerating voltage. The choice of cathode material and voltage directly impacts the system's power draw and beam power; however typical ground EBW systems using 60 kV or 120 kV exceed the Prometheus payload's power budget, necessitating a specialized in-space design. Once emitted, electrons are accelerated toward an anode to create a high-energy electron beam, which is then focused by electromagnetic lenses or electrodes to a precise point, enabling deep, narrow welds with minimal distortion. While most EBW systems require a vacuum chamber to prevent atmospheric interference, Prometheus operates in space and thus eliminates this need, reducing mass and power consumption. [3]

1. Design Considerations

When designing an electron beam gun for space applications, several critical considerations must be addressed to ensure functionality and compatibility with the mission environment. Despite its energy efficiency, Electron Beam Welding requires substantial power, which must be carefully managed within the limited energy budget of the BCT Venus Class bus. The gun's design must also prioritize minimizing mass and complexity due to the payload constraints of space missions. The compact dimensions and weight restrictions necessitate a lightweight gun that can fit onto robotic arms without compromising their maneuverability or structural integrity. Additionally, the electron beam gun must be small enough to integrate seamlessly with the robotic arms tasked with manipulating it during welding operations. The compact design will ensure operational flexibility while maintaining precision in confined areas.

2. Gun Selection

A trade study across multiple notable in-space EBW systems was conducted. The designs included the Skylab M-551 metals experiment, NASA's Universal Hand Tool, the Salyut-7 Versatile Hand Tool [4], and a "new" electron beam gun designed by Boris E. Paton [4,5].

Table 1: Electron Beam Welding Gun Trade Study

	Weight	Goal	Paton Design	Skylab M-551	Universal Hand Tool	Salyut-7 Versatile Hand Tool
Accel. Voltage	20%	Max	10 kV	20 kV	10 kV	5 kV
Normalized Value			0.667	1	0.667	0
Beam Current	20%	Max	250 mA	80 mA	100 mA	100 mA
Normalized Value			1	0	0.1176	0.1176
Beam Power	35%	Max	2.5 kW	1.6 kW	1 kW	0.5 kW
Normalized Value			1	0.55	0.25	0
Dimensions (L/W/H) in mm	10%	Min	220/80/290	400 mm sphere	----	290/135/230
Normalized Value			0	1	----	0.01334
Mass	15%	Min	1.8 kg	20 kg	4.5 kg	3.5 kg
Normalized Value			1	0	0.8516	0.9066
Total			0.8334	0.4925	0.37216	0.160844

Prometheus will select the Paton electron beam welder for its mission due to its lightweight properties and efficient power consumption, making it ideal for space applications where mass and energy are critical constraints. This choice leverages the gun's heritage design by B. E. Paton, who is renowned for his work in space welding technologies. The original design has been successfully ground-tested in simulated space environments, giving it a Technology Readiness Level of 7. The gun is capable of welding aluminum alloys up to 6 mm thick and titanium alloys up to 4 mm thick, more than enough for Prometheus's mission requirements. To adapt this design for the Prometheus system, modifications will be necessary, primarily to remove the handle since the gun will be manipulated by robotic arms instead of being handheld.

The development of the new electron beam gun prioritizes minimizing weight while ensuring high operational reliability. An overview of the electron beam gun is given in Figure 5. During welding, the outer surfaces of the anode unit (1), body (2), and cover (7) are designed to remain below 50°C. In contrast, the cathode component (3) can reach temperatures up to 1800°C. The electrical insulation components, including the Aluminum-Oxide and Kovar contact socket (5), high-voltage insulator (4), and high-voltage input (6), are engineered to withstand the 10 kV accelerating voltage applied during operation. This design both insulates the high temperature gun from the rest of the system and protects it from additional heating from intensive solar emissions, which could cause inconsistencies in weld quality [5].

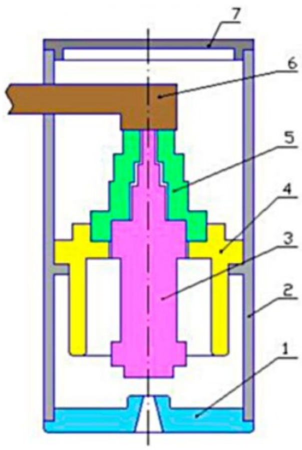

Figure 5. General Arrangement of Electron Beam Gun [5]

3. Gun Analysis

The electron beam gun uses a triode emission system with a lanthanum hexaboride (LaB6) cathode for its high current density and long lifespan. Electron emission is achieved through electron bombardment heating, which requires only 30–40 W—far less than traditional cathode systems. A focusing electrode controls the beam current with high precision, while the anode accelerates electrons to form a focused beam.

The system is designed with optimized electrode geometry to maintain electrical strength and precise beam convergence. The maximum beam current is 250 mA with an accelerating voltage of 10 kV, resulting in a maximum beam power of 2.5 kW.

Using a short-focus configuration, the beam can be focused to a diameter of 0.4 mm, enabling power densities up to 16 kW/mm². This allows for effective welding of most in-space materials, including aluminum up to 6 mm thick and titanium or stainless steel up to 4 mm. The short-focus setup is chosen for Prometheus due to its high precision and controllability. [5]

B. Laser Cutting

The laser cutting system is a crucial component of the Prometheus payload, designed to create flat, uniform surfaces on debris in preparation for welding. The laser cutter will be integrated into the payload for debris mitigation and will operate within it. Mounted on a 3-axis system, it will move like a 3D printer to precisely cut metal.

The payload will utilize a fiber laser, chosen over CO2 & Nd:YAG. A trade study was conducted to select the optimal laser cutting subsystem. It is important to acknowledge that, as of now, no existing fiber laser cutting system is compact enough to be integrated directly into a payload for on-orbit applications. Industrial grade fiber laser cutters capable of performing the necessary operations are not optimized for spacecraft integration.

However, this technological gap does not pose a barrier for the current mission. The Prometheus payload is designed as a proof-of-concept, demonstrating that, *if* a miniaturized space-suitable fiber laser cutting system were to exist, the payload infrastructure and power systems would be fully capable of supporting its operation. This approach ensures that the mission remains valuable when such technology becomes available.

1. Trade Study & Laser Cutter Decision / Analysis

After a comprehensive trade study comparing CO2, fiber, and Nd:YAG laser cutting systems, a fiber laser system was determined to be the optimal choice for the Prometheus payload, based on its superior performance across key criteria for space applications. Fiber lasers offer superior power efficiency, converting 30-50% of electrical energy into usable power [6], compared to 5-20% for CO2 lasers [6] and 20% for Nd:YAG lasers [7]. Additionally, fiber lasers produce a smaller, more focused beam (0.015-0.17mm), enhancing precision for cutting metallic space debris surfaces in preparation for welding, compared CO2 lasers (0.25-0.5mm) and Nd:YAG lasers (2mm) [7].

Fiber lasers outperform in cutting speeds. At 1000W, fiber lasers can cut steel 9m/min 1000W [8], while CO2 lasers are limited to only 3.6m/min with 200W [7]. Nd:YAG lasers achieve 2m/min [9]. Fiber lasers are particularly advantageous for cutting materials like steel and aluminum, which are common in space debris. Fiber lasers also have an operational lifespan of approximately 25,000 hours [10], far surpassing the 1,000-3,000 hours for CO2 lasers [11] and 10,000-15,000 hours for Nd:YAG lasers [9], providing a more reliable long-term solution.

Fiber lasers also produce less excess heat and have a better self-cooling process due to their large surface area to volume ratio, reducing the need for a complex cooling system. Their solid-state design is well-suited for space conditions, providing consistent performance without requiring gas management like CO2 lasers, which are vulnerable to instability in vacuum environments.

2. *Design considerations*

Operating within the payload's strict 444W power limit poses significant challenges, requiring efficient energy management for stable performance. Each photon requires 1.868×10^{-19} J to reach an excited state, necessitating power regulation to light amplification. Power management is supplemented by the DS18 battery, which supports high-demand laser cutting cycles. With a 1250 W-hr capacity, it can sustain approximately 1.85×10^{18} photons per second if full payload power is utilized. A DC-DC power converter is required to amplify wattage, enabling higher energy discharge onto the cutting surface.

To ensure effective heat dissipation in space, active thermal regulation mechanisms such as heat pipes and radiators are employed. Safety measures include reflective coatings on nearby components to minimize heat transfer and protect critical electronics. A continuous fault detection system monitors power levels, temperature, and laser alignment to prevent cascading failures.

3. *Technology Readiness Level & Verification*

The Technology Readiness Level (TRL) of doped fiber laser cutting for space applications remains low despite its widespread use in terrestrial aerospace manufacturing.

While fiber laser cutting has yet to be deployed in ISAM missions, its proven role in aerospace provides a strong foundation for adaptation. Industry leaders such as GE Aviation, GKN Aerospace, and ATK Aerospace Structures utilize fiber lasers to enhance precision and efficiency. GE Aviation integrates fiber lasers with Virtek systems to improve composite fabrication and minimize waste, while GKN Aerospace employs laser projection for faster, more accurate production. Ruag Space collaborates with United Launch Alliance on Vulcan rocket components, and Firefly uses Virtek VPS1 systems for managing complex geometries [7].

These implementations underscore fiber laser cutting's reliability and precision, highlighting its potential for in-orbit applications like debris preparation. Advancing its TRL for space will require research and testing in microgravity, vacuum conditions, and extreme thermal environments.

C. Robotic Arms

The robotic arms subsystem is critical to mission success, the arm must be able to operate in a multitude degree of freedom to manipulate debris and complete the operation of welding. Given its critical nature a trade study of eight robotic arm design that already have been used in-space was conducted, as seen in Figure 6 [12,13,14].

Criteria	Weight	Canadarm2	Dextre	GITAI S1	MDA LMA	Maxar SPIDER	Luna Arm
Mass	10%	2	2	4	4	3	5
Power	10%	2	2	4	4	3	5
Payload Capacity	15%	5	4	3	4	5	2
Range of Motion	15%	4	5	3	4	4	3
Radiation/ Environment Tolerance	10%	5	5	3	4	5	4
Autonomy/ Control Modes	15%	3	4	5	4	5	4
Flight Heritage	10%	5	5	3	3	3	2
Cost & Availability	15%	2	2	5	4	3	5
Total Score	100%	3.4	3.6	3.9	**4.05**	3.85	4

1 = Poor | 3 = Moderate | 5 = Excellent

Figure 6. Robotic Arm Trade Study

While the MDA LMA robotic arm scored the best on the trade study, modifications were needed in order to perform the operations of welding and specialized attachment was needed to be model. Additionally, given the confined volume the payload is provided, the arms needed to be scaled down. Structural supports were also increased to prevent failure during operational phases. Figure 7 depicts the current iteration design of the robotic arm with the welder attachment. The robotic arm with the grabber at the end look similar with the only difference being the end of the arm.

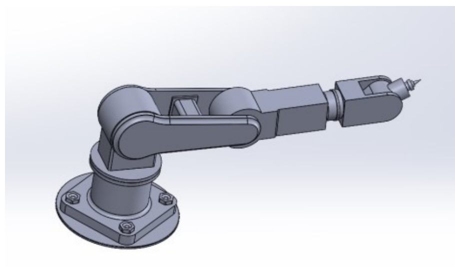

Figure 7. Robotic Welding Arm

D. Structures

The structure of the Prometheus payload will have to fulfil the following requirements for success of the mission. The structure of the payload must be able to withstand the load throughout the mission without failure. The structure must also withstand temperature change throughout the mission without significant deformation. The payload must also be able to withstand possible damage due to debris that could be caused during the welding and laser cutting processes. With these things in mind, a design for the payload was created. By first starting with creating a list of necessary features for the success of the mission, including the folding plate, the robotic arms (one with the electron beam welder and with a grabber), as well as a section of the payload body cut out for the laser cutter, and linear and rotary actuators to enable deployment of the folding plate. The linear actuators and rotary actuators to be used were chosen from a trade study done on each. The linear actuators to be used are Xeryon Lightweight Linear Actuators [15] and the rotary actuators chosen to be used are Xeryon Precision Rotation Stages [16]. Both were chosen due to being lightweight and having low power requirements. From there, an initial CAD was created as shown in Figure 2.

1. Material Selection

Once the CAD was done, a trade study was conducted on three metals that are commonly used for satellites. This included Aluminum 6061-T4, Titanium Ti-6Al-4v, and Stainless Steel SS321. The trade study compared these metals based off density, weldability, Young's Modulus, Ultimate Tensile Strength, Melting Point, and coefficient of Thermal Expansion. The chosen material for the payload was Aluminum 6061-T4 as it is one of the easiest metals to weld, has a high strength to weight ratio which are key to the mission [17].

2. Structural Analysis

After the material was selected, structural analysis could be done to determine whether the payload would be able to withstand that loads throughout the mission. Finite Element Analysis was done using SolidWorks to determine the maximum deformation that the payload would experience. As the maximum load that the payload would undergo would be during launch, an acceleration of 5g's was used to correspond with the launch loads experienced by a payload launching with the chosen Falcon 9 launch vehicle [18]. A fixed boundary condition was placed on the side of the payload where it would be attached to the X-Sat Venus class bus. The payload design was also simplified to remove parts that would be unlikely to fail and to simplify the mesh used. The results of the FEA are shown in Figure 8.

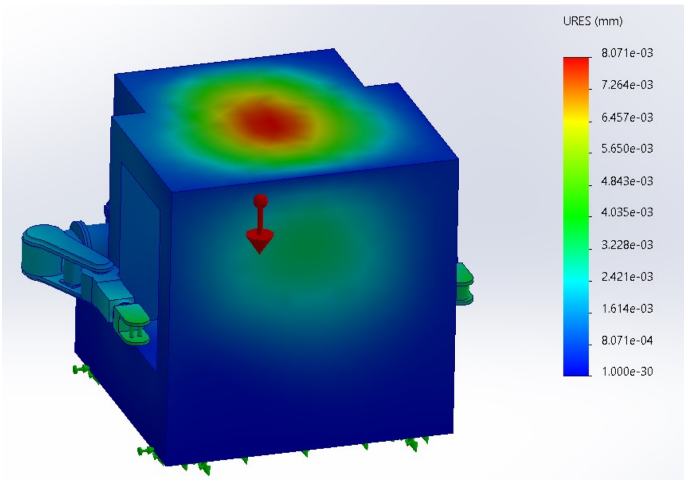

Figure 8. FEA of Launch Loads for the Prometheus Payload

These results show a maximum deformation of 8.071μm which on the scale of the payload does not constitute failure. This shows that the material choice and the overall structural design of the payload meets the top-level requirements for success of the mission.

E. Power

The Prometheus payload faces significant operational challenges due to severe power constraints from welding and laser cutting. Larger batteries are required, but mass limitations prevent their accommodation. As a result, operations must cycle between welding and multiple orbits for recharging, extending mission duration and increasing battery degradation risks. To address these issues, system-level design, analysis, and verification work were conducted to optimize power allocation while ensuring mission feasibility within existing constraints.

1. Design, Analysis & Verification:

Power budget estimation is an iterative process. This analysis references the Firesat mission trade study and the subsystem power allocation table from *Space Mission Analysis and Design (SMAD [19])*. Using a linear regression model from *Elements of Spacecraft Design [20]*, power distribution across the Venus X-class bus and Prometheus payload was determined. Calculations allocated 285 W to the payload and 159 W to the bus, refined further based on subsystem requirements under eclipse and full-illumination conditions.

Table 2. SMAD Subsystem Power Allocation Table [19]

	% of subsystem total			
Subsystem	Comsats	Metsats	Planetary	Other
Thermal control	30	48	28	33
Attitude control	28	19	20	11
Power	16	5	10	2
CDS	19	13	17	15
Communications	0	15	23	30
Propulsion	7	0	1	4
Mechanisms	0	0	1	5

To ensure adequate power supply, the Power Supply Allocation P_{sa} [19] was calculated with a 5% margin over the 444 W incident power from the solar array. Eclipse and illumination power consumption, along with battery efficiencies, X_e & X_i (eclipse and illumination), were analyzed to determine the final P_{sa}.

For a 180-day mission, an STK eclipse report was processed in MATLAB, revealing an average daily eclipse duration of 27,889 seconds and illumination duration of 59,011 seconds. The power allocation process iteratively adjusts subsystem distributions to maintain balance between available solar power and mission demands.

2. Power Allocation

This section summarizes the payload's power distribution. Thermal regulation, command systems, and communications operate with minimal power as the bus facilitates most of those processes. Essential functions are prioritized within the 444W limit, with eclipse efficiency estimated at 75% and daylight at 90%, based on projected technological trends looking 5-10 years into the future. Calculations confirm at P_{sa} of **421.326051W**, ensuring mission feasibility and guiding solar array sizing.

To determine the solar array sizing for the Prometheus payload, key parameters such as inherent degradation, beginning-of-life power, life degradation, and end-of-life power are considered. Inherent degradation, accounting for inefficiencies in solar array assembly, is taken as 0.88 based on SMAD. The beginning-of-life power is calculated to be **390.83 W.**

Over time, solar panels degrade due to thermal cycling. Life degradation, estimated using industry-standard equations, results in a value of **0.986** for the 6-month mission, leading to an end-of-life power of **385.22 W**. Given the minimal degradation, this value remains close to the beginning-of-life power.

Using these parameters, the required solar array area is calculated to be **1.1523 m²** to meet mission power demands while accounting for degradation losses. Additionally, a battery is required to store energy for eclipse periods, with capacity determined based on payload power needs, eclipse duration, depth of discharge, and power transmission efficiency, as detailed in SMAD.

Assuming a power transmission efficiency of 0.9 based on SMAD and a depth of discharge of 0.85, typical for lithium-ion batteries, battery sizing calculations were performed using equations from SMAD, resulting in a required capacity of 1224 Wh. This is necessary to support peak power demands during laser cutting and welding. The payload will use the DS18 INF-35 battery, which weighs 22 lbs and measures 7.71 x 5.15 x 6.53 inches. It has a capacity of 35 Ah at a 10-hour rate to 1.8V per cell, a nominal voltage of 12.8V, and a maximum discharge current of 525A for 5 seconds.

F. Command and Data Handling

The computer requirements for the payload are according to the power budget and that is radiation hardened. Because the payload is mostly autonomous, the computer needs to have enough memory for real-time processing of mission critical objectives, including start/stop times for operations and mission emergencies, for long-term storage for the duration the satellite is not in contact with the ground station, and redundancy and error correction memory for radiation protection. A trade study was conducted on typical computers for small satellites with autonomous operations within the power limit of 30W.

1. Computer Selection

The computers involved are the Xiphos Q7S [21], iXblue Muons [22], and EnduroSat OBC [23]. In this trade study, all these computers are safely within the power budget for C&DH, so the objective is to maximize computer power. For a fully autonomous spacecraft performing ISAM operations with real-time AI decision-making, the more power, the better. In terms of the computer mass, this mission aims to reduce mass for the payload's overall efficiency. The flight history of these computers was also investigated since a thorough flight history will imply a high Technology Readiness Level (TRL). A high TRL incurs less risk to the payload, but since this category has no quantifiable public data on how often these parts were bought and used in space, this was measured binarily for significant in-space reputation of the computer's company.

Table 3. Computer Trade Study

	Weight	Goal	Xiphos Q7s	iXblue Muons	EnduroSat OBC
Power	45%	Max	5-15W	10-20W	1-5W
Normalized Value			0.333	1	0
Mass	35%	Min	32g	60g	130g
Normalized Value			1	0.286	0
Flight History	20%	Max	1	0	1
Total	100%		0.6998	0.5501	0.2

Based on this, the Xiphos Q7S is a clear stand out. This computer is known for its capabilities with high-end AI and manageable power consumption, so it supports the mission beyond the trade study criteria.

2. Data Handling Architecture

The architecture of data handling was also evaluated between centralized architecture, ring architecture, and bus architecture. Because of the number of subsystems sending status messaging to the computer, there is cause for concern about congestion. Conducting a quantitative trade study is difficult for these types of architecture, so a detailed comparison of the benefits and issues between each type was used for architecture down-selection instead.

The ring architecture biggest benefit is redundancy, which is not a concern on this mission. The bus architecture is more accommodating of the numerous subsystems aboard the payload. Many of the mission operating subsystems are in the same location and the bus architecture provides flexibility to accommodate that, unlike a centralized architecture. Prometheus will use SpaceWire for communication protocol on the bus architecture [24]. Figure 9 is a basic block diagram of command and data handling architecture onboard.

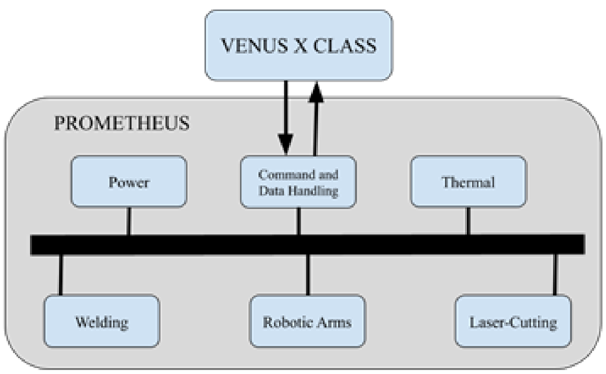

Figure 9. C&DH Block Diagram

G. Mass Budget

Prometheus' mass budget was creating using a bottoms-up approach as detailed in Table 14-20 in the new SMAD. Throughout the design and validation work, a basic top-down approach was used to outline a preliminary percentage breakdown of weight per subsystem, but as the team advanced through part-selection through numerous trade studies, the official mass budget produced here as Table 4 was created. This mass budget puts the payload comfortably below the mass maximum constraints and can therefore support any additional weight from the target debris welding onto the body and any self-generated debris contained during the laser cutting procedure.

Table 4. Prometheus Mass Budget

	TRL	Quantity	Unit Mass [kg]	Total Mass [kg]	% Breakdown
Thermal				4	8.66%

C&DH					
Computer	9	1	0.032	0.032	0.07%
Wiring	9	0.75	0.087	0.06525	0.14%
Battery					
Battery	4	2	10	20	43.28%
Converter	4	2	1.322	2.644	5.72%
Structure					
Linear Actuators	7	2	0.0055	0.011	0.02%
Rotational Actuators	6	2	0.45	0.9	1.95%
EBW	8	1	1.8	1.8	3.90%
Grabbing Hands	1	2	0.04	0.08	0.17%
Base Payload	9	1	16.68	16.68	36.09%
				46.21225	100.00%

IV. Host Spacecraft Integration and Mission Analysis

Outside of the Prometheus Payload, decisions need to be made about the launch vehicles, ground stations, and the X-sat Venus Class bus. The following shows a detailed description of the work done on these to integrate them into the Prometheus mission.

A. Launch Vehicle

The launch vehicle to be used for the Prometheus Mission was determined by conduction a trade study to compare the SpaceX Falcon 9, the Rocket Lab Electron, and the Relativity Terran 1. These launch vehicles were compared based on reusability, reliability, Payload Mass capacity to LEO, ESPA Ring compatibility, and the estimated cost. The launch vehicle that was chosen was the SpaceX Falcon 9. This is a 2-stage liquid propelled rocket. The Falcon 9 had a superior payload mass allowance for LEO of 22,800 kg allowing for ride share decreasing the price [18, 25]. The Falcon 9 is also reliable as it has completed 446 missions. One of these missions include the ispace-U.S.'s Mission 3 which launched two Venus class satellites using the SpaceX Falcon 9 showing that it can be used for missions similar to Prometheus [26, 27]. The first stage of the Falcon 9 rocket consists of nine Merlin engines which create 7607 kN of thrust at sea level and 8227 kN of thrust in a vacuum. This stage also has landing legs which allow for the rocket to land on Earth and be reused. The second stage has one Merline Vacuum engine which creates 981 kN of thrust in a vacuum. The payload fairing of the SpaceX falcon has a height of 13.1 m and diameter of 5.2 m is large enough to fit the Prometheus payload and accompanying Venus Class Bus [18, 25].

The launch site must be able to support the inclination that is needed to rendezvous with the piece of space debris. The DELTA 1 DEB space debris that was chosen for this mission has an inclination of 101.8 degrees [28]. The possible launch sites were limited to those in the US, as this will decrease costs in transportation of the launch system since the Falcon 9 is built in the US, and to those that can achieve the 101.8-degree inclination of the DELTA 1 DEB space debris. This leaves the Vandenberg Air Force Base in California, United State as the only option for a launch site as it has the capability of launching the Falcon 9 and can support the necessary inclination [29].

B. Ground Stations

To determine the ground stations needed for the Prometheus mission, the piece of debris that the payload would rendezvous with needed to be determined. DELTA 1 DEB was the debris selected for the Prometheus mission. The orbit for DELTA 1 DEB was then plotted in Ansys Systems Tool Kit (STK). Originally, three ground stations were selected that lay on the path of the DELTA 1 DEB: Abu Dhabi Leolut, Clewiston, and Tidbinbilla.

Due to power constraints and the fact that the Prometheus payload doesn't have much information to communicate to the ground, only one ground station is going to be used. To determine which of the ground stations to use, a trade study was performed using the number of debris passes over the ground station per week, the minimum payload contact duration, maximum payload contact duration, and average payload contact duration as evaluation criteria.

The Abu Dhabi Leolut ground station had the highest minimum payload contact duration, maximum payload contact duration, and average payload contact duration while still having a high number of debris passes per week. The required data rate for the Prometheus mission was 17 Mbps, and the Abu Dhabi Leolut ground station can handle data rates of 2.5 Gbps which is much more than necessary. This is why the Abu Dhabi Leolut ground station was selected to be the ground station for the Prometheus mission.

C. Communications

Communication to and from the ground station will happen via the Venus Class Bus. Autonomy at this level greatly decreases the constraints on the orbit path Prometheus takes, allowing for this mission to be used for different pieces of debris without intense restraint on debris location.

Information about mission operations will be handled from the payload to the bus and downlinked from the bus. The bus will only receive an initial activation command from the ground station. When the bus passes over Abu Dhabi, raw mission critical data which includes start/stop times for operations and mission emergencies are downlinked. Once mission operations are complete, final data about the quality of the weld will also be downlinked.

To create a link budget for the downlinked data, the frequency was determined from the ground station and the transmitter power was divided from power allotted to the communication subsystem. Abu Dhabi's ground station frequency is 1.5 GHz, and from the SMAD Table 13-10 [19], this frequency sets the system noise temperature as 221K. Abu Dhabi's receiving antenna has a 2.3m diameter with a 1.2 degree pointing error [30].

The bus will equip an antenna with low power consumption and accommodating frequencies. The bus will use the AAC SpaceQuest ANT-100 [31] static whip antenna from the same manufacturer as the computer used aboard the payload. This antenna can be made with a diameter of 20".

For the uplink, there is an S-band frequency with a smaller transmitter power compared to the downlink. Since there is little data being sent to the bus or payload for the duration of the mission, little power is needed for this section. Half of the downlink transmitter power is considered in the uplink budget. Again, from the SMAD Table 16 determines the system noise temperature is 614K.

Table 1. Simplified Uplink and Downlink Budget

Commented [KB1]: Insert title for table

	Downlink	Uplink
Frequency [GHz]	1.5	2.0
Xmtr. Power [W]	0.5	0.3
Bitrate [Mbps]	5.26	5.09
Link Margin [dB]	10.17	7.80

D. Guidance, Navigation, and Control

The Venus X Class bus will determine its own attitude using multiple different sensors including gyroscopes, magnetometers, and a sun sensor. The bus will determine its attitude by fusing the different sensor inputs into an extended Kalman filter. Cameras will be attached to the payload to provide information on how to orient the robotic arms to grab and manipulate the debris. After the spacecraft determines its attitude, the bus will be able to control itself to achieve the desired orientation of the payload and robotic arms.

To determine the proper controls for the Venus X Class bus, different categories of controls were investigated. Stability theory-based control methods, optimization theory-based control methods, and AI-based control methods were researched to determine which method would be best for the Prometheus mission.

A trade study was conducted on the different types of control methods with algorithmic flexibility, algorithmic efficiency, and algorithmic stability and robustness as evaluation criteria. Algorithmic flexibility is an algorithm's ability to deal with changing conditions and inputs. Algorithmic efficiency is an algorithm's ability to efficiently complete its task. Algorithmic stability and robustness are an algorithm's ability to get similar results from small perturbations in inputs [32].

AI based methods were chosen for the Prometheus mission because of the efficiency and flexibility they provide. AI control methods are already effective means of control, but they are still relatively new methods. There is a lot of room left for development in AI control methods, meaning that the controls on the Prometheus payload can become even more efficient in the next few years.

E. Orbital Analysis

The piece of debris selected for the Prometheus mission is the DELTA 1 DEB. The Prometheus payload will rendezvous with this debris and remain on its orbit throughout the mission's lifecycle. The orbit for DELTA 1 DEB was plotted in STK and the orbital elements were determined. The semi-major axis of the orbit is 7500 km, eccentricity is 0.005618, and orbital period is 107.73 min.

F. Structures

The approximate size of the X-sat Venus Class bus was determined by comparing photographs of the bus provided by Blue Canyon Technologies to the person that was put next to it as reference. The approximate size of the X-sat Venus class bus was determined to be 33 in x 33 in x 18 in, the structure can be approximated to be a rectangular shell with thickness 3/8 in. This was then put into a CAD model and FEA was then used to simulate how the Venus Class Bus could withstand the forces of launch (which is the largest force the Venus Class bus would experience). Once again this was tested at 5 g's of acceleration which would be experienced due to the SpaceX Falcon 9 [18]. One side of the payload which would be attached to the ESPA ring was set to the fixed boundary condition. In Figure 0, the results of the FEA are shown.

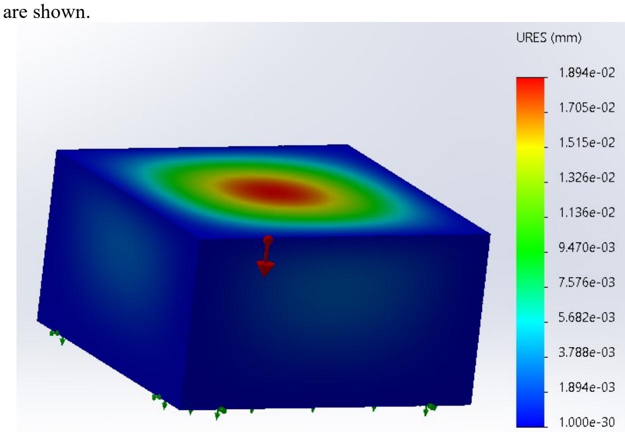

Figure 10. FEA of X-Sat Venus Class Bus During Launch

The maximum deformation shown is 18.94 μm which compared to the scale of the bus. This value for deformation does not constitute failure of the spacecraft.

G. Thermal

Thermal control system for the Prometheus mission consists of a combination of passive and active components, designed to maintain thermal balance with minimized complexity. Figure 11 [33] below illustrates the cold (left) and hot (right) cases that are experienced by CubeSat class satellites when analyzed as a single-node.

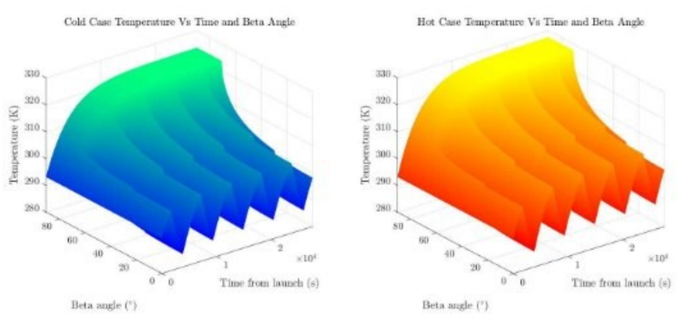

Figure 11. Hot and Cold Temperature Cases for CubeSat Class Satellite (Single-node)

Understanding these hot and cold temperatures cases leads to the design of the thermal control system. Starting with coatings, Table 6 [34] are some of the option available for selection as an exterior coating. Choosing options that offer similar absorption and emissivity values allow for the payload to operate either extreme hot or cold conditions.

Table 6. Thermal Coatings Absorption and Emissivity

	Aeroglaze Z306	Carbon NS-7	N-150-1	Beryllium Copper	Hughson L-300	384 ESH* UV
Absorption	0.96	0.96	0.94	0.92	0.95	0.97
Emissivity	0.91	0.88	0.94	0.72	0.84	0.75

Aeroglaze Z306 offers absorption and emissivity values that are similar to each other, making it the preferred coating option for this payload.

Active components of the thermal control system will consist of radiators and heaters, working in tandem to regulate internal payload component temperatures. Ideal thermal control system will regulate the internal payload temperature to range between -10 to 60 degrees Celsius.

V. Risks and Fault Recovery/De-Scope Options

Prometheus is a technology demonstration mission that aims to improve autonomous ISAM capabilities in the scope of welding and laser cutting. As such, the mission design accepted risks associated with low TRL technologies. Specific high risks for Prometheus are detailed in Table 72. The table explains the mission mitigation methods for each risk and how the mitigation affects severity and likelihood of each risk. Highly critical risks, like a threat to Prometheus' structural integrity, have extreme mitigation strategies already integrated into the design, like risk 2.1. The decision to add in a compartment for self-generated debris caused by the mission's operations was necessary to effectively address debris mitigation beyond welding debris to the body. For high consequence low probability risks, redundant systems are in place to mitigate consequences.

Prometheus is able to diagnose failure during the critical operations involving capture, laser cutting, and welding and consistently monitors power and temperature levels. In the event of an autonomy failure, a manual override contingency can be given via override commands from the ground station. If the payload completely fails, the VENUS X-Class Bus will remain operational and will continue to be in contact with ground station, since the communication and GNC systems are housed in the Bus. Overall, the payload's design reflects a proactive approach to operational integrity, failure management, and debris migitation. These mitigation strategies have decreased the risks associated with the mission, which can be seen in Figure 12, a colored risk matrix with mitigation strategies mapped also.

Table 72. Risk Mitigation Matrix

Risks	Severity	Likelihood	Mitigation Strategy	Severity	Likelihood
1. Autonomy Fail	Severe	Possible	Manual Override Contingency	Minor	Very Unlikely
2. Hit Debris					
2.1 Self-generated Debris	Severe	Very Likely	Contain laser cutting and welding procedures inside the payload	Moderate	Unlikely
2.2 External Debris	Significant	Likely	Rendezvous with isolated piece of debris	Significant	Unlikely
3. Insufficient Battery Charge	Moderate	Likely	Add additional battery	Moderate	Very Unlikely
4. Overheated internal parts	Severe	Moderate	Increase radiation hardening and thermal coverage near laser and welding arm	Severe	Unlikely
5. Low TRL	Moderate	Very Likely	Additional component testing with in-space conditions	Minor	Possible

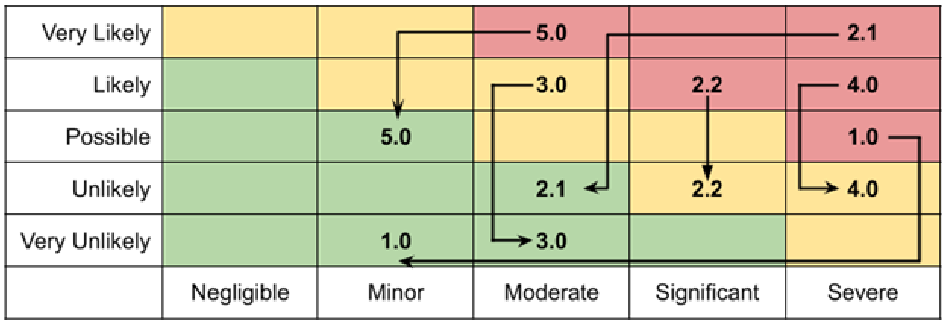

Figure 12. Risk Mitigation Matrix

VI. Future Work

In the future, the Prometheus mission will need innovations to be made to improve the technology currently available for the success of the mission. This mission involves using some technology that currently exists but needs to be scaled down for use on this mission. Vision-based algorithms need to be implemented into the payload to help with debris rendezvous. Knowing the location of the debris will allow for algorithms that control the movements of the robotic arms to perform the payload maneuvers autonomously. More in-depth thermal analysis should also be done to better understand the flow of heat due to the laser cutter and the electron beam welder. This must be done after a scaled down version of the laser cutter and electron beam welder is made.

Further work must also be done to improve the debris mitigation efforts for the laser cutting and welding operations. The Prometheus mission will do laser cutting inside the payload to aid in the mitigation efforts and use electron beam welding as it creates the lowest amount of debris. While these efforts will decrease the debris generation of the mission, further work still needs to be done to improve debris mitigation. This mission hopes to use debris to weld, and laser cut in the hopes of reusing debris instead of creating more.

A more detailed description of the internal wiring of the payload must also be done. Currently, the equipment to be used on the Prometheus payload has been chosen but a detailed determination of how each will be interconnected has yet to be performed. A more detailed determination of the thermal control system must be done to determine where coatings, radiators, and heaters must be placed.

VII. References

[1] “Space Environment Statistics · Space Debris User Portal.” Retrieved 10 April 2025. https://sdup.esoc.esa.int/discosweb/statistics/

[2] COSMIC. *2024 COSMIC Capstone Challenge – Information Packet.* COSMIC-E01-WD001-2024-A, July 10, 2024.

[3] P N, Siddharth & Sathiya Narayanan, Chinnaiyan. (2020). A review on Electron Beam Welding process. Journal of Physics: Conference Series. 1706. 012208. 10.1088/1742-6596/1706/1/012208.

[4] N. Naden and T.J. Prater, "A Review of Welding in Space and Related Technologies," NASA TM-2020-220557, 2020.

[5] B.E. Paton et al., "New Electron Beam Gun for Welding in Space," Science and Technology of Welding and Joining, Vol. 24, No. 4, pp. 1-7, 2018.

[6] “Fiber vs. Nd:YAG Laser Cutting Machine - Which Is Better?,” STYLECNC, Mar 07 2016. Retrieved 18 March 2025. https://www.stylecnc.com/industry-news/Fiber-laser-cutting-machine-VS-YAG-laser-cutting-machine.html

[7] “Applications of fiber laser cutting machines in aerospace manufacturing - ADH machine tool,” *ADH Shop* Available: https://shop.adhmt.com/applications-of-fiber-laser-cutting-machines-in-aerospace-manufacturing/.

[8] “UPGRADE YAG TO FIBER LASER,” The Manufacturer of Fiber Laser Cutting Machine. Retrieved 18 March 2025. https://gyclaser.com/support/upgrade-yag-to-fiber-laser/.

[9] “Space Grade Nd:YAG,” Teledyne FLIR. https://www.flir.com/products/space-grade-ndyag/?vertical=surveillance+general&segment=surveillance#:~:text=Teledyne%20FLIR’s%20radiation%20hardened%20%E2%80%9CSpace,Osiris%2DRex%20(NASA).

[10] Laserax, “Fiber Lasers: Everything You Need to Know,” Laserax, Nov 26 2020. Retrieved 18 March 2025. https://www.laserax.com/blog/fiber-laser.

[11] “CO2 Laser Vs. Fiber Laser: The Main Differences.” Retrieved 18 March 2025. https://www.xometry.com/resources/sheet/co2-laser-vs-fiber-laser/.

[12] “Pittsburgh Aerospace Company: Astrobotic Technology,” *Astrobotic* Available: https://www.astrobotic.com/.
[13]“On-orbit servicing, assembly, and manufacturing 1 (OSAM-1),” *NASA* Available: https://www.nasa.gov/mission/on-orbit-servicing-assembly-and-manufacturing-1/.
[14] “ISAM service,” *GITAI* Available: https://gitai.tech/isam-service/.
[15] “Xeryon Launches the World’s Smallest 78 Nanometer Precision Actuator | RoboticsTomorrow.” Retrieved 17 March 2025. https://roboticstomorrow.com/news/2021/06/07/xeryon-launches-the-worlds-smallest-78-nanometer-precision-actuator/16976/
[16] “XRT Ultrasonic Rotation Stage,” Xeryon. Retrieved 17 March 2025. https://xeryon.com/products/precision-rotation-stages/xrt-ultrasonic-rotation-stage/.
[17] Material, W., “Aluminum 6061, Al 6061-T6 Alloy Properties, Density, Tensile & Yield Strength, Thermal Conductivity, Modulus of Elasticity, Welding,” World Material. Retrieved 4 March 2025. https://www.theworldmaterial.com/al-6061-t6-aluminum-alloy/.
[18] “Falcon 9 Launch Vehicle Payload User’s Guide,” SpaceX, 2009. https://spaceflightnow.com/falcon9/001/f9guide.pdf.
[19] Larson, W J and Wertz, J R. "Space Mission Analysis and Design." , Jan. 1992. Larson, W J, & Wertz, J R (1992)
[20] Brown, C. D., “Elements of Spacecraft Design,” American Institute of Aeronautics and Astronautics, Inc, Reston, Va, 2002.
[21] “Xiphos Flight Computer Processor,” AAC Clyde Space. Retrieved 27 Feb 2025. https://www.aac-clyde.space/what-we-do/space-products-components/command-data-handling/q7s?.
[22] “Product Range,” Excail. Retrieved 27 Feb 2025. https://www.exail.com/product-range.
[23] “Onboard Computer,” Endurosat. Retrived 27 Feb 2025. https://www.endurosat.com/products/onboard-computer/
[24] “An Overview of the SpaceWire Standard,” STAR-Dundee. Retrieved 6 Mar 2025. https://www.star-dundee.com/spacewire/getting-started/an-overview-of-the-spacewire-standard/.
[25] “Falcon 9,” SpaceX. Retrieved 3 March 2025. https://www.spacex.com/vehicles/falcon-9/.
[26] Casey, M., “Ispace-U.S. to Use RTX’s Blue Canyon Technologies Spacecraft Bus for Lunar Far Side Communications Relay Satellites,” ispace U.S., Apr 09 2024. Retrieved 3 March 2025. https://ispace-us.com/2024/04/ispace-u-s-to-use-rtxs-blue-canyon-technologies-spacecraft-bus-for-lunar-far-side-communications-relay-satellites/.
[27] “Ispace Releases Updates on Progress of Mission 2 and Mission 3,” ispace. Retrieved 3 March 2025. https://ispace-inc.com/news-en/?p=4401.
[28] “DELTA 1 DEB Satellite Details 1967-006D NORAD 2707.” Retrieved 16 March 2025. https://www.n2yo.com/satellite/?s=2707#google_vignette.
[29] “Of Inclinations and Azimuths,” The Planetary Society. Retrieved 16 March 2025. https://www.planetary.org/articles/3450.
[30] “LEOLUT Antenna and Ground Station,” Honeywell. Retrieved 18 Feb 2025. https://automation.honeywell.com/us/en/products/more-products/search-and-rescue/leolut-600
[31] “ANT-100,” AAC Clyde Space. Retrieved 25 Feb 2025. https://www.aac-clyde.space/what-we-do/space-products-components/communications/ant-100
[32] Chai, R., Tsourdos, A., Savvaris, A., Chai, S., Xia, Y., and Chen, C. L. P., “Review of Advanced Guidance and control algorithms for space/aerospace vehicles,” Progress in Aerospace Sciences Available: https://www.sciencedirect.com/science/article/pii/S0376042121000014.
[33] Versteeg, C., and Cotten, D. L., *Preliminary thermal analysis of small satellites* Available: https://s3vi.ndc.nasa.gov/ssri-kb/static/resources/Preliminary_Thermal_Analysis_of_Small_Satellites.pdf.
[34] *NASA* Available: https://ntrs.nasa.gov/api/citations/19840015630/downloads/19840015630.pdf.